



Catalytic Role of HI in the Interstellar Synthesis of Complex Organic Molecule

Shuming Yang¹, Peng Xie², Enwei Liang¹, and Zhao Wang¹

¹Laboratory for Relativistic Astrophysics, Department of Physics, Guangxi University, Nanning 530004, China; zw@gxu.edu.cn

²School of Chemistry and Chemical Engineering, Guangxi University, Nanning 530004, China

Received 2022 November 28; revised 2023 March 2; accepted 2023 March 21; published 2023 April 28

Abstract

Using quantum chemical calculations, we model the pathways for synthesizing two purine nucleobases, adenine and guanine, in the gas-phase interstellar environment, surrounded by neutral atomic hydrogen (HI). HI is found active in facilitating a series of fundamental proton transfer processes of organic synthesis, including bond formation, cyclization, dehydrogenation, and H migration. The reactive potential barriers were significantly reduced in the alternative pathways created by HI, leading to a remarkable increase in the reaction rate. The presence of HI also lowered the reactive activation temperature from 757.8 K to 131.5–147.0 K, indicating the thermodynamic feasibility of these pathways in star-forming regions where some of the reactants have been astronomically detected. Our findings suggest that HI may serve as an effective catalyst for interstellar organic synthesis.

Key words: astrochemistry – astrobiology – ISM: molecules

1. Introduction

Finding the synthesis pathways of interstellar complex organic molecules (COMs) of biological interest is paramount for explaining the origin of the elementary building blocks of life detected on meteorites, comets and asteroids (Burton et al. 2012; Singh et al. 2013; Misra et al. 2017; Morse & Chan 2019). The formation of biomolecules through direct collisions between abiotic molecules is generally challenging in the cold environment of the interstellar medium (ISM). Photochemical and radiation chemical processes, particularly on ice/dust grains, are commonly regarded as the principal steps toward synthesizing interstellar COMs (Herbst & Van Dishoeck 2009; Öberg 2016; Materese et al. 2020; Carrascosa et al. 2021; Mifsud et al. 2021). While the ion-neutral or radical routes are the commonly considered mechanisms for the gas-phase synthesis of interstellar COMs, catalyzed reactions are emerging as alternative processes since the majority of the detected interstellar molecules are neutral and have a closed shell.

Catalysts, often in the form of free radicals, ions, or metal clusters, are frequently utilized in laboratory experiments of organic chemistry to convert a challenging molecule–molecule reaction into a more straightforward molecule–radical or radical–radical reaction (Qin et al. 2017; Zhao et al. 2020). For the synthesis of interstellar organics, previous works suggest that ice/dust grains, hydronium, and carbamic acid could function as catalysts (Mendoza et al. 2004; Roy et al. 2007; Rimola et al. 2012; Saladino et al. 2013; Vinogradoff et al. 2015; da Silva & de Araujo 2017; Qi et al. 2018;

Potapov et al. 2019; Hanine et al. 2020). For example, radicals such as $\cdot\text{NH}_2$ and $\cdot\text{CN}$ are considered to participate the reactions for synthesizing nucleobases from HCN, and are capable of reducing the barrier and may even render some reactions barrierless (Jeilani et al. 2013, 2016). Nonetheless, the low abundance of the previously suggested catalysts often renders the catalyzed reaction seemingly impossible in ISM, as it requires the collision of three bodies. Fortunately, this is not always the case. If the concentration of the catalyst is in great excess of that of the reactants, the reaction can occur just as easily as a two-body collision. Neutral atomic hydrogen (HI) is the simplest and the most abundant free radical in the universe. It dominates the chemical composition of the ISM, and is virtually ubiquitous in every interstellar environment. In hot molecular cores, the concentration of HI is about 7–10 orders of magnitude higher than that of COMs (Herbst & Van Dishoeck 2009).

Although HI is a common reactant or product in simple interstellar reactions, its catalytic activity in interstellar organic synthesis remains unclear in most astrochemistry models (Bergantini et al. 2014; Singh et al. 2014; Fedoseev et al. 2015; Chuang et al. 2016; Fedoseev et al. 2016; Misra et al. 2017; Carrascosa et al. 2020; Slate et al. 2020; Miksch et al. 2021). In comparison to its molecular form, atomic hydrogen is rare on Earth and is difficult to prepare and control in laboratory experiments. As a result, quantum chemical calculations are expected to shed light on whether HI plays a crucial role in the interstellar formation of COMs (Zamirri et al. 2019). Aiming at this question, we conducted a new series of

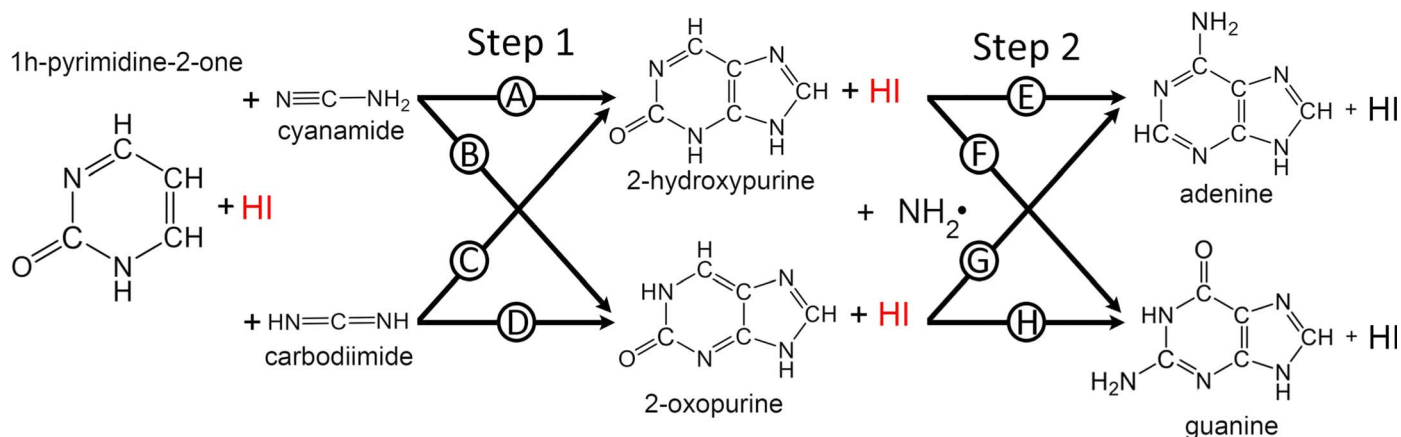


Figure 1. Formation scheme of Ade and Gua.

ab initio quantum chemical calculations to explore the potential catalytic activities of HI in the formation pathways of adenine (Ade) and guanine (Gua).

Ade and Gua are two purine nucleobases constituting the genetic code in the nucleic acids. After having been detected in meteorites, their extraterrestrial origin and prebiotic formation are a long-debated focus of attention in attempts to answer the abiogenesis question (Peeters et al. 2003; Burton et al. 2012). Intensive efforts are therefore devoted to find the synthesis pathways of nucleobases in laboratory experiments simulating the chemical evolution of abiotic molecules in interstellar environments (Glaser et al. 2007; Gupta et al. 2011; Merz et al. 2014; Parker et al. 2015; Chuang et al. 2016; Fedoseev et al. 2016; Bera et al. 2017; da Silva & de Araujo 2017; Parker & Kaiser 2017; Sandford et al. 2020; Choe 2021; Fulvio et al. 2021). In particular, Ade, Gua and purine derivatives have been synthesized through photochemical reactions of purine in an interstellar ice analog (Materese et al. 2017, 2018). 2-aminopurine and isoguanine are assumed to be two key intermediates for these reactions. Nevertheless, the HI-catalyzed synthesis of nucleobases has yet to be investigated.

2. Methods

We consider novel synthesis pathways of Ade and Gua starting from 1h-pyrimidine-2-one C₄H₄N₂O, a direct intermediate toward nucleobases produced by two interstellar molecules: formamide H₂NCHO and vinyl cyanide H₂CCHCN (Lu et al. 2021). Our proposed pathways involve two steps, illustrated in Figure 1. In the 1st step (via the paths A-D), C₄H₄N₂O reacts with either cyanamide (NH₂CN) or carbodiimide (HNCNH) (both detected in Sgr B2 and Orion-KL (Turner et al. 1975; White et al. 2003; McGuire et al. 2012; Belloche et al. 2013) to form two direct purine-base precursors, 2-hydroxypurine (C₅H₄N₄O) and 2-oxopurine (C₅H₄N₄O), via the paths A-D. In the 2nd step, these two precursors produce

Ade or Gua by separately reacting with ·NH₂ via the paths E-H. We focus on the catalytic activities of HI in the both steps.

Multiple possible collision trajectories were simulated for each reaction pathway. The transitional and final molecular structures in single molecular collision events were determined by structural optimization using first principles calculations (Barone et al. 2015; Maeda et al. 2015; Zamirri et al. 2019; Pan et al. 2021; Puzzarini 2022), in which the system's total potential is minimized in the framework of the density functional theory (DFT) at M06-2X/6-31+G(d,p) level as implemented in Gaussian 16 B.01 (Frisch et al. 2016). We chose this level of theory in view of its proven records of accuracy in predicting physical chemical properties of relevant compounds (Mardirossian & Head-Gordon 2017; de Jesus et al. 2021). In our previous work (Lu et al. 2021), this method was compared with calculations based on Møller Plesset perturbation theory in the second order (MP2), and a good agreement was achieved.

Vibration frequency calculations were here carried out to confirm the intermediate (IM) and the transition state (TS). Intrinsic reaction coordinate (IRC) calculations were performed to ensure that the TS reasonably connect the reactant (RC) and the product (PD). To incorporate HI in our calculations, we initially positioned a HI in a transition state with the reactant. We then performed IRC coordinate scanning to ensure that the HI molecule's placement was appropriate. Subsequently, we simulated multiple trajectories of collisions between the HI and the reactant from various positions. A static calculation is used for this step, unlike what occurs in molecular dynamics (Wang 2019, 2020). Finally, we selected trajectories with the lowest energy cost to facilitate the reaction. The atomic coordinate data of all optimized molecular structures, including RC, IM, TS, and PD, are provided in the standard XYZ chemical file format in the Supplementary Information's Data section.

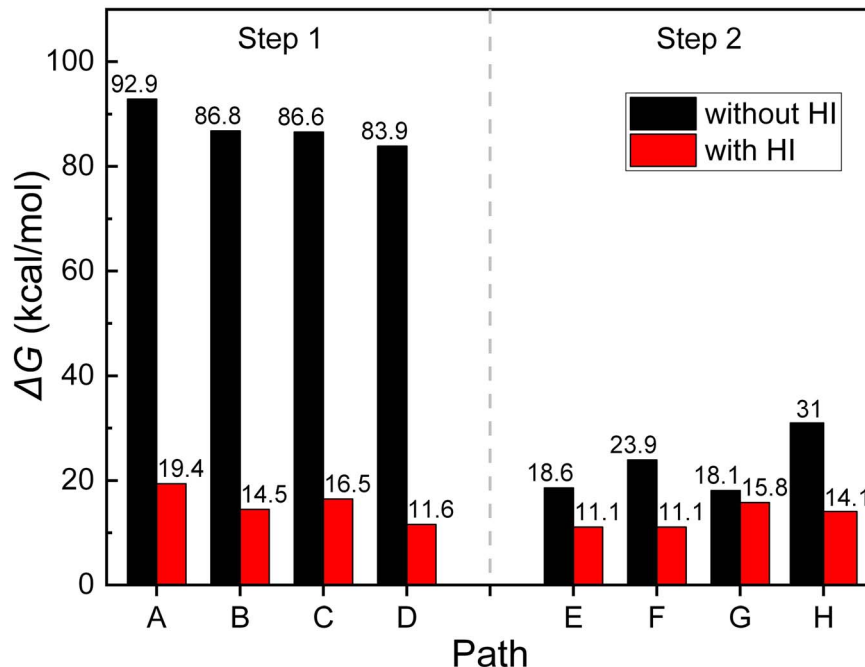


Figure 2. Minimum reactive potential barrier for different reaction paths.

The Gibbs free energy G was calculated for every optimized structure of RC, IM, TS or PD at a thermodynamic temperature of 150 K under the assumption of non-interacting particles (McQuarrie & Simon 1999) (p321–325). This representative temperature corresponds to a typical temperature of hot molecular cores. The potential barrier ΔG of a reaction pathway was determined as the difference in G between the highest-energy states (including IM, TS, or PD) and the RC in each of the two steps described in Figure 1. This definition of the reactive barrier assumes that the energy does not leave the system by irradiation on a timescales typical of the atomic rearrangements, which is in general much faster than the needed vibration cascade. As multiple collision trajectories were simulated for each path, only the energetically favorable trajectories with the lowest ΔG are discussed in the following section.

3. Results and Discussions

The reactive barrier ΔG is a crucial parameter for assessing the feasibility and significance of a reaction in the ISM, as it strongly correlates with the reaction rate and activation temperature. Figure 2 displays the minimum energy costs of producing Ade and Gua from $C_4H_4N_2O$ through various paths, and compares ΔG for reactions with (red bars) and without (black bars) the involvement of HI. The results demonstrate that HI greatly promotes the reactions.

In the absence of HI, the reaction pathway (Path A-D, left half) shows a high barrier with $\Delta G > 83 \text{ kcal mol}^{-1}$, which is

expected since the fused pyrimidine-imidazole rings in Ade and Gua are complex to synthesize without a catalyst. However, the addition of HI significantly facilitates the reactions, reducing ΔG to $11.6\text{--}19.4 \text{ kcal mol}^{-1}$. Path D, involving HNCNH, shows the lowest barrier among the proposed paths, indicating that it is more active than its isomer NH_2CN . Considering steps 1 and 2 consecutively, the optimal pathway is either Paths B + G/D + G or D + H, with HI as a catalyst. The corresponding optimal barrier for synthesizing Ade or Gua is around 15.8 or $14.1 \text{ kcal mol}^{-1}$, respectively.

As the temperature of a gas rises, its constituent molecules collide more frequently and with greater kinetic energy. As a result, the fraction of collisions that can surmount the barrier ΔG increases, following the Arrhenius relation. In chemical kinetics, the Eyring–Polanyi equation (Eyring 1935) describes the relationship between the reaction rate constant k , ΔG , and T ,

$$k = \frac{C\kappa_B T}{h} e^{-\frac{\Delta G}{RT}}. \quad (1)$$

where C is the transmission coefficient, κ_B is the Boltzmann constant, R is the molar gas constant, and h is the Planck constant. Using this equation, we estimate k as a function of T as plotted in Figure 3, for the optimal reactive paths of Ade and Gua with and without HI. Generally speaking, many significant reactions in the ISM typically proceed with a rate constant of $10^{-11} \text{ cm}^3 \text{ s}^{-1}$ or larger (above the dashed horizontal orange line). Without catalyst, such a rate constant

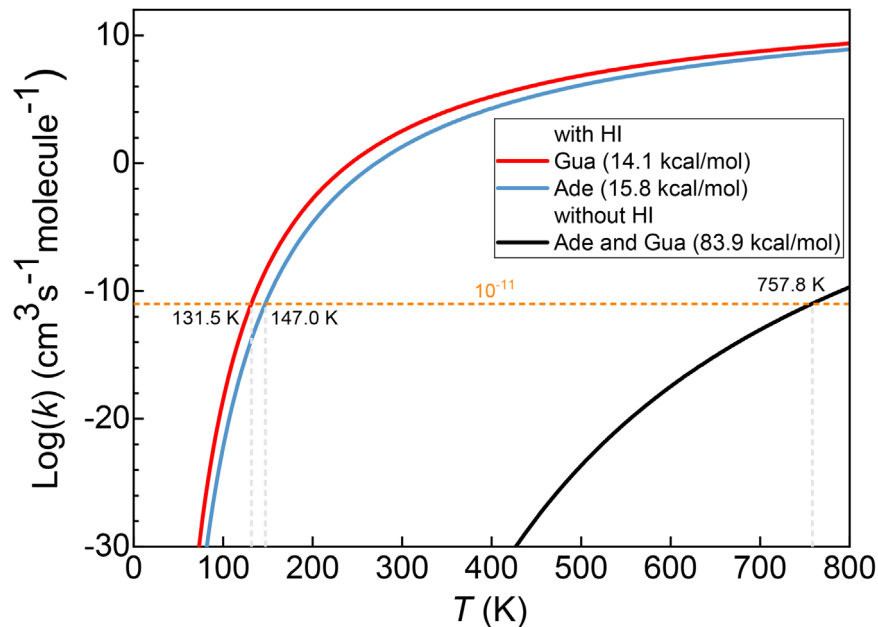


Figure 3. Reaction rate constant vs. temperature for the optimal paths without (black curve) and with H I (red and blue curves). The ternary reactions with H I are assumed to be pseudo binary reactions.

would roughly require a reactive temperature >757.8 K with $\Delta G = 83.9$ kcal mol $^{-1}$, as indicated by the dashed line intersecting with the black curve in Figure 3. The feasibility of such a reaction would be low in the generally cold, gas-phase environment of dense molecular clouds, as the reactants would have to coincide with radiation having an appropriate amount of energy at the time of collision. In contrast, the presence of H I significantly accelerates the reaction, leading to a substantial increase in the reaction rate constant by approximately 20–30 orders of magnitude (as seen in Figure 3). As a result, the required activation temperature is respectively reduced to only 131.5 or 147.0 K for Gua or Ade, as indicated by the dashed lines intersecting with the red and blue curves. To verify our computational model, we compute the half-life time based on the reaction rate and compare it to the results of Zamirri et al. (2019), with agreement obtained as shown in Part I of the Supplementary Information.

Three-body collision processes are often deemed impossible in the ISM, but this does not hold true for the H I-catalyzed reaction. This is because the concentration of H I vastly exceeds that of COMs, reaching 10^7 – 10^{10} times in hot cores (Herbst & Van Dishoeck 2009). Thus, ternary reactions with H I are essentially pseudo-binary reactions. In chemistry models for star-forming regions, the H I abundance is estimated to be comparable to that of H₂ (Garrod et al. 2008; Sun & Du 2022). In addition to the remaining background H I from large-scale molecular clouds, H I also stems from the photodissociation of H₂ by the radiation emitted from young stellar objects (YSOs). This in particular points to the inner parts of protoplanetary

disks, in which the ultraviolet radiation can be dramatically enhanced and resulting in a chemical structure resembling that of a photon-dominated region (van Dishoeck et al. 2006). In such a region, photons are usually not energetic enough to ionize hydrogen but can dissociate molecular hydrogen (Hollenbach & Tielens 1999). For example, the total H I mass in a protoplanetary disk is estimated to be $11.4 M_{\text{Earth}}$ with a typical vertical column density of 1.7×10^{21} or 3.3×10^{20} cm $^{-2}$ at 5 or 110 au, respectively (Kamp et al. 2008). Moreover, H I is a common product of many important reactions in ISM (Herbst & Klemperer 1973), as proton transfer is a fundamental process in organic reaction (Mayer 2011).

The involvement of H I makes the proposed pathways thermally feasible in certain interstellar environments with low activation temperatures. For instance, the formation sites of YSO are often associated with warm ambient gas, known as hot cores or corinos, with average temperatures up to 300 K, where a rich organic chemistry is observed (Herbst & Van Dishoeck 2009; Jørgensen et al. 2020). Interestingly, most of here-used reactants, including NH₂CHO, CH₂CHCN, NH₂CN, and HNCNH, are detected to co-exist in SgrB2 and Orion KL hot cores (Turner et al. 1975; White et al. 2003; McGuire et al. 2012; Belloche et al. 2013; Scibelli et al. 2021). Note that the reactant C₄H₄N₂O is supposed to be synthesized from NH₂CHO and CH₂CHCN (Lu et al. 2021), which are also both detected in those regions as “hot” molecules with characteristic rotation temperature >100 K (Belloche et al. 2013; López et al. 2014; Fu & Lin 2016; Suzuki et al. 2018;

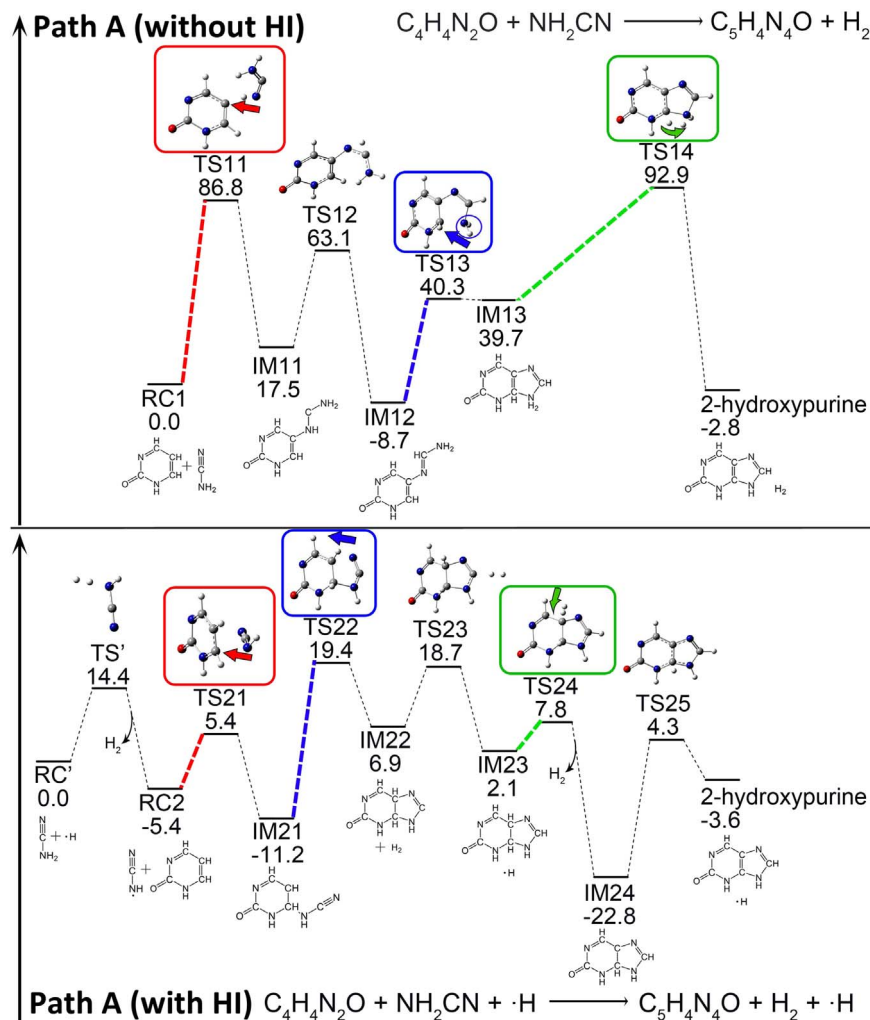


Figure 4. Potential energy surface for forming 2-hydroxypurine ($C_5H_4N_4O$) from $C_4H_4N_2O$ and NH_2CN in via Path A without (upper panel) or with H I (lower panel). The arrows indicate the direction of molecular collision.

Lopez-Sepulcre et al. 2019). Those regions contain the initial materials as well as enough thermal energy for the proposed reactions to proceed. It is noteworthy that protoplanetary disks are also of particular interest for abiogenesis, as the planets formed in them inherit their chemical compositions. Although only simple organics have been detected in protoplanetary disks so far (Öberg & Bergin 2021), the activation temperature reported in this study for nucleobase synthesis is lower than that in the inner part of disks, as the temperature gradually increases from 10 K to several thousand K from the outer layer to the central forming star (Akimkin et al. 2013).

One might naturally inquire about the specific effects of H I in promoting the reaction. To showcase the catalytic capabilities of H I, Figure 4 provides a comparison of the reaction pathways in the absence and presence of H I, using path A as an example. H I is found to facilitate several critical processes,

including cyclization, dehydrogenation, and the bonding of the reactants. In the absence of H I, the reaction is impeded by a significant barrier of $86.8 \text{ kcal mol}^{-1}$ against the formation of an initial bond between the two reactants (see the step in the red line, upper panel). However, when H I is present in the vicinity, it can extract a hydrogen atom from the amino group with a relatively low cost of only $14.4 \text{ kcal mol}^{-1}$, converting NH_2CN into the highly reactive HNCN radical. This generates an alternative pathway in which the barrier for bonding the two reactants is considerably lowered to $10.8 \text{ kcal mol}^{-1}$, as indicated by the red line in the lower panel.

In path A, the rate determining step involves two conventional organic synthesis processes, namely cyclization and dehydrogenation. Initially, cyclization exhibits a high barrier of around $49.0 \text{ kcal mol}^{-1}$, as indicated by the blue circle in the upper panel of Figure 4. This barrier arises because the N end

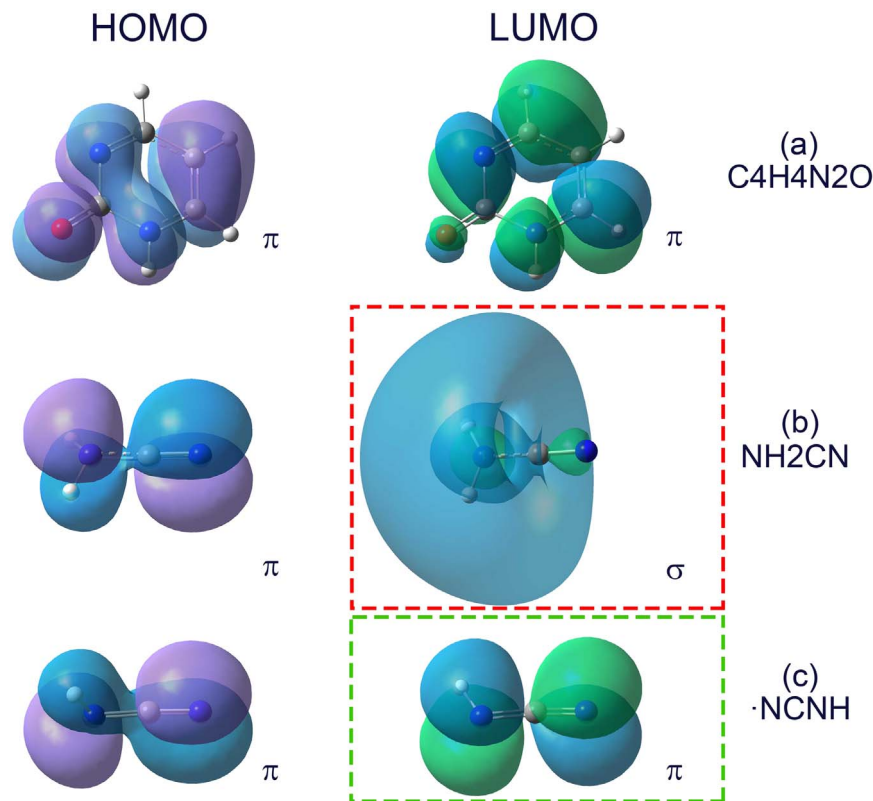


Figure 5. HOMO (left) and LUMO (right) of C₄H₄N₂O (a), NH₂CN (b), HNCN (c).

required for forming the imidazole ring is completely saturated. However, this process is expedited in the alternative pathway created by HI, where the (1h-pyrimidine-2-one-6-yl)-cyana-mide radical (IM21) possesses an unsaturated N end, as depicted by the blue rectangle in the lower panel of Figure 4. Although cyclization still requires approximately 30.6 kcal mol⁻¹, the energy retained in the preceding sub-steps helps to surmount this barrier, owing to the low energy of IM21.

The next step is dehydrogenation, in which a C-bonded and an N-bonded hydrogen atom in the imidazole ring are converted into a H₂ molecule, resulting in the formation of 2-hydroxypurine C₅H₄N₄O, as shown in Figure 4. The original barrier for this process is roughly 53.2 kcal mol⁻¹, which is substantially reduced in the alternative pathway created by HI in the lower panel (green line). One of the H atoms in IM23 is taken by the free HI, at a small cost of only 5.7 kcal mol⁻¹, to generate the stable IM24, 1,6-dihydro-purin-2-one radical. This radical ultimately yields 2-hydroxypurine (C₅H₄N₄O) by directly removing another H atom.

The catalytic activity of HI is demonstrated using the initial step of Path A in Figure 4 as an example within the framework of the frontier molecular orbital theory. This step involves the formation of a bond between the reactants, C₄H₄N₂O and

NH₂CN, to initiate the reaction. However, because the highest occupied molecular orbital (HOMO) of C₄H₄N₂O (located on the left in Figure 5(a)) and the lowest unoccupied molecular orbital (LUMO) of NH₂CN (outlined in red) have mismatched symmetry (π versus σ orbital), a high energy is required to form the bond. The feasibility of a reaction process is closely related to the conservation of orbital symmetry, and a lack of symmetry can impede the reaction (Woodward & Hoffmann 1965, 1969). Consequently, a significant HOMO-LUMO gap of 7.1 kcal mol⁻¹ arises, making the reaction difficult to proceed. Fortunately, HI has the ability to extract a hydrogen atom from NH₂CN, thereby transforming it into a radical HNCN, which can readily initiate the reaction because its LUMO symmetry (outlined in green) is consistent with the HOMO symmetry of C₄H₄N₂O (π versus π orbital). As a result, the HOMO-LUMO gap is significantly reduced to 3.6 kcal mol⁻¹, allowing for the reaction to proceed smoothly.

HI has also been found to aid in hydrogen migration, as demonstrated in Path H, where 2-oxopurine (C₅H₄N₄O) reacts with ·NH₂ to form Gua, as depicted in Figure 6. To initiate this reaction, a proton must move from an N site to an adjacent O site, which requires approximately 31.0 kcal mol⁻¹ (see yellow line in the upper panel). This barrier can be reduced by the presence of HI, which binds to the relevant O atom, creating a

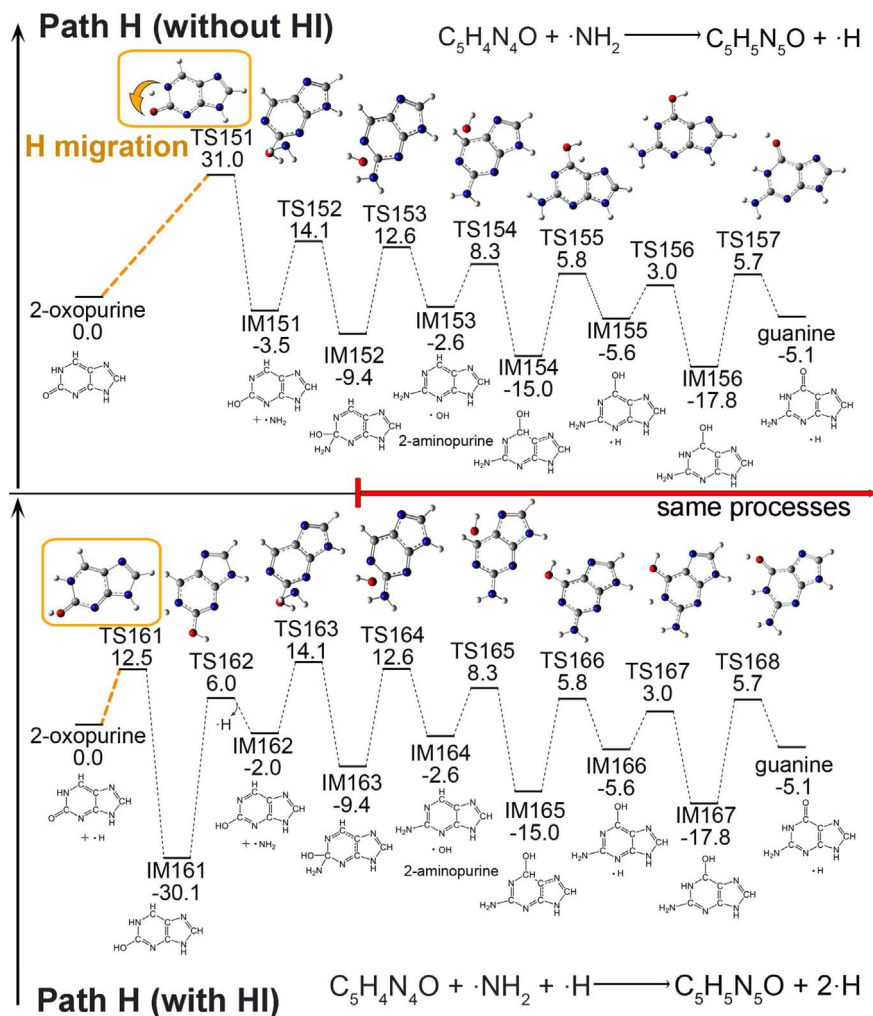


Figure 6. Potential energy surface to form Gua from 2-oxopurine ($C_5H_4N_4O$) and $\cdot NH_2$ via Path H without (upper) or with HI (lower). The processes in the two paths become the same after IM152 and IM163.

highly stable intermediate, IM161, 2-hydroxy-3H-Purine radical, as shown in the lower panel. This intermediate sits in a deep potential well, and the energy that it contains aids in overcoming the subsequent processes of dehydrogenation and bonding between $\cdot NH_2$ and a sp^2 -hybridized C.

The catalytic effects of HI are observed in all of the simulated reaction paths (B-G), as provided in Part II of the Supplementary Information. Additionally, several stable intermediates are identified in the proposed reaction pathways, including 2-aminopurine, purinol, 2-hydroxypurine, 2-oxopurine, and isoguanine. Some of these intermediates align with the findings of prior laboratory experiments. For instance, 2-aminopurine (IM153 or IM164 in Figure 6) was discovered by Materese et al. (2017, 2018) in a photochemistry experiment on an interstellar ice analog and was believed to be a critical intermediate in the synthesis of Ade, Gua, and purine

derivatives. The results of this experiment also suggest the same function for isoguanine and purinol. The present study elucidates the pathways from these intermediates to the purine bases. Finally, the IR and electronic adsorption spectra of these key intermediates are calculated using DFT calculations (Kovács et al. 2020; Meng et al. 2021; Wu et al. 2022) and are presented in Part III of the Supplementary Information to facilitate potential astronomical observations.

4. Conclusions

The proposed new pathways for the synthesis of Ade and Gua demonstrate the efficiency of HI as a catalyst in promoting various fundamental organic synthesis processes, including bond formation, cyclization, dehydrogenation, and H migration. These are typical proton transfer processes in organic synthesis, where HI can effectively lower the potential barrier

and significantly increase the reaction rate constant by up to 20–30 orders of magnitude, depending on the temperature. As a result, the activation temperature required for the proposed reaction is lowered from 757.8 to 131.5–147.0 K when HI is present. This suggests that the thermal feasibility of gas-phase purine base synthesis with HI could be possible in environments such as hot molecular cores or protoplanetary disks. From a broader perspective, given the prevalence of HI as a major component of interstellar gas and the fundamental role of proton transfer in organic synthesis, the HI-catalyst mechanism should have wide implications for the formation of organic molecules in the ISM.

Acknowledgments

This work was supported by the National Natural Science Foundation of China (11964002).

References

- Akimkin, V., Zhukovska, S., Wiebe, D., et al. 2013, *ApJ*, **766**, 8
- Barone, V., Biczysko, M., & Puzzarini, C. 2015, *AcChR*, **48**, 1413
- Belloche, A., Müller, H. S., Menten, K. M., Schilke, P., & Comito, C. 2013, *A&A*, **559**, A47
- Bera, P. P., Stein, T., Head-Gordon, M., & Lee, T. J. 2017, *AsBio*, **17**, 771
- Bergantini, A., Pilling, S., Rothard, H., Boduch, P., & Andrade, D. 2014, *MNRAS*, **437**, 2720
- Burton, A. S., Stern, J. C., Elsila, J. E., Glavin, D. P., & Dworkin, J. P. 2012, *Chem Soc Rev*, **41**, 5459
- Carrascosa, H., Cruz-Díaz, G., Muñoz Caro, G. M., Dartois, E., & Chen, Y. 2020, *MNRAS*, **493**, 821
- Carrascosa, H., González Díaz, C., Muñoz Caro, G., Gómez, P., & Sanz, M. L. 2021, *MNRAS*, **506**, 791
- Choe, J. C. 2021, *ApJ*, **914**, 136
- Chuang, K.-J., Fedoseev, G., Ioppolo, S., Van Dishoeck, E., & Linnartz, H. 2016, *MNRAS*, **455**, 1702
- da Silva, J. B. P., & de Araujo, A. P. M. 2017, *ESC*, **1**, 376
- de Jesus, D. N., da Silva, J. M., Tejero, T. N., et al. 2021, *MNRAS*, **501**, 1202
- Eyring, H. 1935, *JChPh*, **3**, 107
- Fedoseev, G., Chuang, K.-J., van Dishoeck, E. F., Ioppolo, S., & Linnartz, H. 2016, *MNRAS*, **460**, 4297
- Fedoseev, G., Cuppen, H. M., Ioppolo, S., Lamberts, T., & Linnartz, H. 2015, *MNRAS*, **448**, 1288
- Frisch, M. J., Trucks, G. W., Schlegel, H. B., et al. 2016, Gaussian Inc 16 vB.01 (Wallingford, CT: Gaussian Inc)
- Fu, L., & Lin, G.-M. 2016, *RAA*, **16**, 182
- Fulvio, D., Potapov, A., He, J., & Henning, T. 2021, *Life*, **11**, 568
- Garrod, R. T., Weaver, S. L. W., & Herbst, E. 2008, *ApJ*, **682**, 283
- Glaser, R., Hodgen, B., Farrelly, D., & McKee, E. 2007, *AsBio*, **7**, 455
- Gupta, V., Tandon, P., Rawat, P., Singh, R., & Singh, A. 2011, *A&A*, **528**, A129
- Hanine, M., Meng, Z., Lu, S., et al. 2020, *ApJ*, **900**, 188
- Herbst, E., & Klemperer, W. 1973, *ApJ*, **185**, 505
- Herbst, E., & Van Dishoeck, E. F. 2009, *ARA&A*, **47**, 427
- Hollenbach, D. J., & Tielens, A. 1999, *RvMP*, **71**, 173
- Jeilani, Y. A., Nguyen, H. T., Newallo, D., Dimandja, J.-M. D., & Nguyen, M. T. 2013, *PCCP*, **15**, 21084
- Jeilani, Y. A., Williams, P. N., Walton, S., & Nguyen, M. T. 2016, *PCCP*, **18**, 20177
- Jørgensen, J. K., Belloche, A., & Garrod, R. T. 2020, *ARA&A*, **58**, 727
- Kamp, I., Freudling, W., Robberto, M., Chengalur, J., & Keto, E. 2008, *PhysS*, **2008**, 014013
- Kovács, P., Zhu, X., Carrete, J., Madsen, G. K., & Wang, Z. 2020, *ApJ*, **902**, 100
- López, A., Tercero1, B., Kisiel, Z., et al. 2014, *A&A*, **572**, A44
- Lopez-Sepulcre, A., Balucani, N., Ceccarelli, C., et al. 2019, *ESC*, **3**, 2122
- Lu, S., Meng, Z., Xie, P., Liang, E., & Wang, Z. 2021, *A&A*, **656**, A84
- Maeda, S., Harabuchi, Y., Ono, Y., Taketsugu, T., & Morokuma, K. 2015, *IJQC*, **115**, 258
- Mardirossian, N., & Head-Gordon, M. 2017, *MolPh*, **115**, 2315
- Materese, C. K., Gerakines, P. A., & Hudson, R. L. 2020, *AcChR*, **54**, 280
- Materese, C. K., Nuevo, M., McDowell, B. L., Buffo, C. E., & Sandford, S. A. 2018, *ApJ*, **864**, 44
- Materese, C. K., Nuevo, M., & Sandford, S. A. 2017, *AsBio*, **17**, 761
- Mayer, J. M. 2011, *AcChR*, **44**, 36
- McGuire, B. A., Loomis, R. A., Charness, C. M., et al. 2012, *ApJL*, **758**, L33
- McQuarrie, D. A., & Simon, J. D. 1999, *Molecular Thermodynamics* (Mill Valley, CA: Univ. Science Books) (Sterling Publishing Company)
- Mendoza, C., Ruetter, F., Martorell, G., & Rodriguez, L. 2004, *ApJL*, **601**, L59
- Meng, Z., Zhu, X., Kovács, P., Liang, E., & Wang, Z. 2021, *ApJ*, **922**, 101
- Merz, K. M., Jr., Aguiar, E. C., & da Silva, J. B. P. 2014, *JPCA*, **118**, 3637
- Mifsud, D. V., Hailey, P. A., Muiña, A. T., et al. 2021, *FrASS*, **8**, 757619
- Miksch, A. M., Riffelt, A., Oliveira, R., Kästner, J., & Molpeceres, G. 2021, *MNRAS*, **505**, 3157
- Morse, A. D., & Chan, Q. H. 2019, *ESC*, **3**, 1773
- Öberg, K., I 2016, *ChRv*, **116**, 9631
- Öberg, K., I, & Bergin, E. A. 2021, *PhR*, **893**, 1
- Pan, L., Carrete, J., & Wang, Z. 2021, *JPCM*, **34**, 015303
- Parker, D. S., & Kaiser, R. I. 2017, *ChSRv*, **46**, 452
- Parker, D. S., Kaiser, R. I., Kostko, O., et al. 2015, *ApJ*, **803**, 53
- Peeters, Z., Botta, O., Charnley, S., Ruitkamp, R., & Ehrenfreund, P. 2003, *ApJL*, **593**, L129
- Potapov, A., Theulé, P., Jäger, C., & Henning, T. 2019, *ApJL*, **878**, L20
- Puzzarini, C. 2022, *FrASS*, **8**, 252
- Qi, H., Picaud, S., Devel, M., Liang, E., & Wang, Z. 2018, *ApJ*, **867**, 133
- Qin, Y., Zhu, L., & Luo, S. 2017, *ChRv*, **117**, 9433
- Rimola, A., Sodupe, M., & Ugliengo, P. 2012, *ApJ*, **754**, 24
- Roy, D., Najafian, K., & von Ragué Schleyer, P. 2007, *PNAS*, **104**, 17272
- Saladino, R., Botta, G., Delfino, M., & Di Mauro, E. 2013, *ChEurJ*, **19**, 16916
- Sandford, S. A., Nuevo, M., Bera, P. P., & Lee, T. J. 2020, *ChRv*, **120**, 4616
- Scibelli, S., Shirley, Y., Vasyunin, A., & Launhardt, R. 2021, *MNRAS*, **504**, 5754
- Shivani, Misra, A., & Tandon, P. 2017, *RAA*, **17**, 1
- Singh, A., Misra, A., Tandon, P., et al. 2013, *RAA*, **13**, 912
- Singh, A., Misra, A., Tandon, P., et al. 2014, *RAA*, **14**, 275
- Slate, E. C., Barker, R., Euesden, R. T., Revels, M. R., & Meijer, A. J. 2020, *MNRAS*, **497**, 5413
- Sun, J., & Du, F. 2022, *RAA*, **22**, 065022
- Suzuki, T., Ohishi, M., Saito, M., et al. 2018, *ApJS*, **237**, 3
- Turner, B., Liszt, H., Kaifu, N., & Kisliakov, A. 1975, *ApJL*, **201**, L149
- van Dishoeck, E. F., Jonkheid, B., & van Hemert, M. C. 2006, *FaDi*, **133**, 231
- Vinogradoff, V., Duvernay, F., Fray, N., et al. 2015, *ApJL*, **809**, L18
- Wang, Z. 2019, *JPCC*, **123**, 15166
- Wang, Z. 2020, *JPCC*, **124**, 3851
- White, G. J., Araki, M., Greaves, J., Ohishi, M., & Higginbottom, N. 2003, *A&A*, **407**, 589
- Woodward, R. B., & Hoffmann, R. 1965, *JChS*, **87**, 395
- Woodward, R. B., & Hoffmann, R. 1969, *AngCh Int*, **8**, 781
- Wu, R.-Q., Long, M.-Q., Zhang, X.-J., et al. 2022, *RAA*, **22**, 035014
- Zamirri, L., Ugliengo, P., Ceccarelli, C., & Rimola, A. 2019, *ESC*, **3**, 1499
- Zhao, L., Kaiser, R. I., Lu, W., et al. 2020, *AngChIE*, **59**, 11334